AFRL-AFOSR-VA-TR-2021-0071

A Comprehensive Study of Shock-wave-boundary-layer Interactions on Curved Surfaces

Rajan Kumar
Florida Agricultural and Mechanical University Tallahassee
1500 Wahnish Way
Tallahassee, FL, 32307-3100
US

07/08/2021
Final Technical Report

DISTRIBUTION A: Distribution approved for public release.

Air Force Research Laboratory
Air Force Office of Scientific Research
Arlington, Virginia 22203
Air Force Materiel Command

REPORT DOCUMENTATION PAGE	*Form Approved* *OMB No. 0704-0188*

1. REPORT DATE *(DD-MM-YYYY)*	**2. REPORT TYPE**	**3. DATES COVERED** *(From - To)*
08-07-2021	Final	15 Jul 2017 - 14 Jan 2021

4. TITLE AND SUBTITLE
A Comprehensive Study of Shock-wave-boundary-layer Interactions on Curved Surfaces

5a. CONTRACT NUMBER

5b. GRANT NUMBER
FA9550-17-1-0269

5c. PROGRAM ELEMENT NUMBER
61102F

6. AUTHOR(S)
Rajan Kumar

5d. PROJECT NUMBER

5e. TASK NUMBER

5f. WORK UNIT NUMBER

7. PERFORMING ORGANIZATION NAME(S) AND ADDRESS(ES)
Florida Agricultural and Mechanical University Tallahassee
1500 Wahnish Way
Tallahassee, FL 32307-3100
US

8. PERFORMING ORGANIZATION REPORT NUMBER

9. SPONSORING/MONITORING AGENCY NAME(S) AND ADDRESS(ES)
AF Office of Scientific Research
875 N. Randolph St. Room 3112
Arlington, VA 22203

10. SPONSOR/MONITOR'S ACRONYM(S)
AFRL/AFOSR RTA1

11. SPONSOR/MONITOR'S REPORT NUMBER(S)
AFRL-AFOSR-VA-TR-2021-0071

12. DISTRIBUTION/AVAILABILITY STATEMENT
A Distribution Unlimited: PB Public Release

13. SUPPLEMENTARY NOTES

14. ABSTRACT
This was submitted at the original reporting requirement date but was somehow lost. The PI sent me the attached report.

15. SUBJECT TERMS

16. SECURITY CLASSIFICATION OF:			**17. LIMITATION OF ABSTRACT**	**18. NUMBER OF PAGES**	**19a. NAME OF RESPONSIBLE PERSON**
a. REPORT	**b. ABSTRACT**	**c. THIS PAGE**			SARAH POPKIN
U	U	U	UU	15	**19b. TELEPHONE NUMBER** *(Include area code)* 000-0000

DISTRIBUTION A: Distribution approved for public release.

<u>Final Report</u>

Submitted to

Air Force Office of Scientific Research

A Comprehensive Study of Shock-Wave-Boundary-Layer Interactions on Curved Surfaces

AFOSR Grant # FA9550-17-1-0269

AFOSR Program Manager
Dr. Sarah Popkin
Program Manager, Aerothermodynamics
Air Force Office of Scientific Research
Email: sarah.popkin@us.af.mil

HBCU/MI Program Point of Contact
Mr. Edward Lee
Air Force Office of Scientific Research
Email: edward.lee@us.af.mil

Submitted by
Dr. Rajan Kumar
Department of Mechanical Engineering
FAMU-FSU College of Engineering
Tallahassee, FL 32310
Email: rkumar@eng.famu.fsu.edu

In Collaboration with
Dr. Timothy Eymann
DoD HPCMP CREATE Program, Kestrel Team
AFRL/RQHP

1. Executive Summary

A comprehensive study involving experiments and numerical simulations was carried out to understand the flow physics associated with shock boundary layer interactions and shock-shock interactions on an axisymmetric configuration. The shock interaction mechanisms on an axisymmetric body with a curved surface are very complex and different than conventionally studied two and three-dimensional configurations involving flat surfaces. In the present study, the experiments were carried out at the FAMU-FSU College of engineering polysonic wind tunnel and numerical simulations were performed by AFRL- RQHP team using Kestrel flow solver. Kestrel, a multi-physics flow solver, is the fixed wing component of the Computational Research and Engineering Acquisition Tools and Environments (CREATE) Program managed by the Department of Defense High-Performance Computing Modernization Program (DoD HPCMP). Measurements include flow visualizations using surface oil flow and high-speed shadowgraph, surface static pressures using Electronic Pressure Scanner (ESP), surface static pressure field using Pressure Sensitive Paint (PSP) technique, unsteady pressure distributions using fast-response Kulite pressure sensors and force measurements using a six-component strain gage balance. Results show that shock emanating from the wedge impinges on and wraps around the body leading to crossflow separation and reattachment. The flow features observed are very different from the well-documented 2/3D canonical configurations involving SBLI on flat surfaces. The separation bubble grows non-linearly in size with the smallest in length at the top generator (the side facing the shock generator). There is no well-defined length scale in this interaction. Surface pressure distributions obtained using ESP, PSP and Kestrel match very well, and show some interesting results. The narrowband spectra show low-frequency oscillations at the shock impingement and the interaction region. Shock impingement alters the aerodynamic characteristics of the axisymmetric body, generating a pitch-up or pitch-down behavior depending on the shock location with respect to the center of pressure.

2. Introduction and Objectives

Shock Wave Boundary Layer Interactions (SBLIs) exist on both internal and external surfaces of a supersonic/hypersonic flight vehicle. In a typical supersonic engine inlet, compression of the incoming air is achieved through multiple oblique shock waves, which then interact with the boundary layer on an opposing or adjacent surface. Shock waves originating from the aircraft nose or wing leading edge impinge on the external surfaces of stores released from the parent aircraft. These interactions result in flow separation, vortical structure formation, pressure losses, induced pitching moments, and are often detrimental to the operation of the vehicle. The SBLI phenomena are highly unsteady and reduce propulsion efficiency, control surface effectiveness, and undesirable change in vehicle trajectory, and induce an unanticipated structural response. In hypersonic flight, SBLIs has the potential to cause localized surface heating that can destroy a vehicle.

The flow physics associated with SBLI has been thoroughly studied on the two-dimensional canonical configurations. Extensive experimental investigations revealed accurate and useful correlations to enable prediction of flow separation and attachment, the length of the separation bubble and associated dynamics for configurations including normal/ oblique shock interaction, the compression ramp, and the compression-expansion ramp. The three-dimensional canonical configurations that have been exploited are single-fin, swept ramp and double fin. The mean flow fields for these 3-D configurations are reasonably well understood, and attempts are currently underway to develop scaling laws and understand the underlying mechanisms responsible for 3-D SBLIs. The main distinction between 2-D and 3-D flows is the nature of the separation zone. In the case of 2-D flows, there is well-defined separation and reattachment lines and the separation bubble dynamics are associated with the bubble length and the reverse flow, whereas in 3-D flows the separated shear layer never attaches, and there is significant spanwise flow velocity. Both in the case of a single fin and swept ramp, there is no reverse flow and the separation is open with its size varying along the span. In the case of the double fin, the sidewalls and corner vortices contaminate the flow even in the symmetry plane, and there is no well-defined separation zone.

The SBLIs become highly complex and the flow mechanisms are likely far different from the much-studied 2-D and 3-D cases if the interaction surface is curved involving surface pressure gradients and three-dimensional as opposed to flat features as contrasted in Figure 1. For example, in the case of a shock impingement on an axisymmetric body at small angles of incidence, the incoming boundary layer is thin, the SBLI is weak, and the flow is attached. At high angles of incidence, the incoming boundary layer on the leeward side is relatively thick, leading to strong SBLIs and separation. Due to the complex nature of this class of flows, most of the previous studies concentrated on canonical 2-D and 3-D configurations involving flat surfaces. The flow physics that remains unknown at this stage is for the case in which the SBLI induced separation on surfaces involving large curvature behaves like 2D separation with a closed separation bubble and associated low-frequency dynamics or open separation as observed in a few 3D SBLI configurations. Some of the practical applications for such a flowfield are supersonic aircraft wing – store interactions, multiple - store separation from an aircraft, missile sub-munitions, and launch vehicle booster separations. In all of these examples, the shock impingement from protuberances on other parts of the vehicle could result in problems related to heat transfer, stability, control, or aerodynamics, which could materially affect the performance of the body in question. To guide the design and control of future flight vehicles it is therefore very important to understand the aero/thermodynamic effects of the SBLIs on curved surfaces.

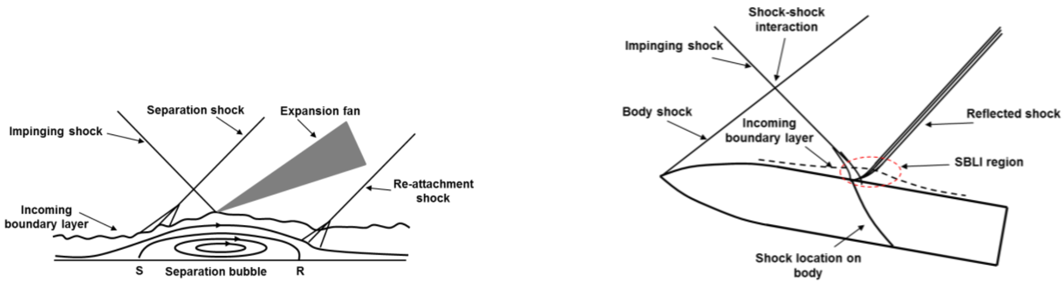

a) Flat plate SBLI b) Axisymmetric body SBLI

Figure 1: *Shock wave boundary layer interactions on canonical configurations.*

To understand the flow physics associated with SBLI on curved surfaces, Computational Fluid Dynamics (CFD) simulations are required to complement the experimental investigations. Kestrel, a multi-physics flow solver, is the fixed wing component of the Computational Research and Engineering Acquisition Tools and Environments (CREATE) Program managed by the Department of Defense High-Performance Computing Modernization Program (DoD HPCMP). Kestrel has recently introduced SAMCart, a Cartesian solver with adaptive mesh refinement, making it possible to simulate and capture the shock system, requires refinement with high fidelity validation data. Once fully functional, Kestrel will serve as an ideal tool for the calculations of shock dominated flows for a variety of DoD applications. In the present study, our goal is to generate much needed fundamental underlying physics and fluid dynamics of SBLI and SSI associated with axisymmetric bodies involving curved surfaces and 3D features.

3. Experiments

3.1 Experimental Facility

The experiments were carried out at the FAMU-FSU polysonic wind tunnel (Fig. 2). The facility has a 12-in x 12-in cross-section, capable of operating in the Mach number regime of 0.2 to 5 including transonic speeds. It produces a unit Reynolds number of 30 million/ft and features two separate test sections: 1) a 12-in x 12-in x 24-in test section with solid walls for sub/supersonic Mach number testing, and 2) a 12-in x 12-in x 48-in section with slotted walls for testing in the transonic speed regime. The polysonic wind tunnel is designed to produce excellent flow quality, an important requirement for the present study. This is achieved through a 10:1 inlet contraction ratio, five fine mesh flow conditioning screens, flow straightener and a settling chamber acoustic treatment. The wind tunnel is equipped with the required instrumentation and flow diagnostic capabilities for the proposed research. This facility allows us to cover a large range of the main interaction parameters, such as Mach and Reynolds number. The test setup includes an ogive cone cylinder body of diameter 1-in and slenderness ratio of 10, and a 10° wedge as a shock generator, as shown in Fig. 2. The shock generator is be mounted to the tunnel ceiling so that the shock impingement location on the ogive body can be varied. The angle of attack of the body was kept constant in these experiments. Measurements were carried out at Mach 2.0.

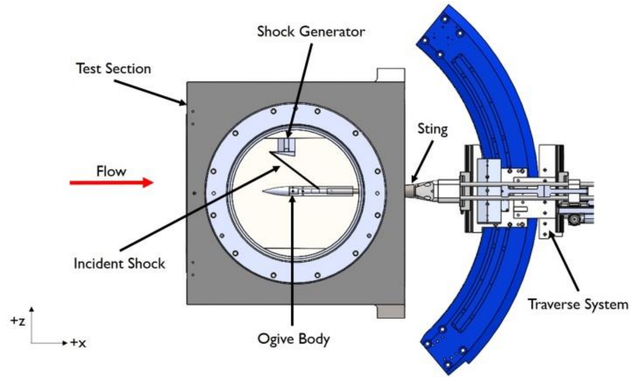

Figure 2. *The FAMU-FSU 12-in x 12-in square cross-section Polysonic wind tunnel and experimental setup****.***

3.2 Measurement Techniques

The experimental setup utilized a wedge-shaped shock generator and an ogive cylinder body model with a slenderness ratio of 10. The ogive nose had a sharp tip which prevented the formation of a bow-shock and ensured the development of an oblique shock. The incoming boundary layer was tripped using 0.10mm grit sand near the tip of the ogive nose. The shock generating wedge, mounted to the ceiling of the supersonic test, had a span of 6 inches and 10-degree turn angle used to generate the planar shock that impinged on the ogive body. Two test models with a tangent ogive nose and different cylindrical bodies were used for testing. Test model-1 contained 16 static pressure ports placed in a helical orientation along the surface of the model. Each port was offset axially $x/D = 0.15$-in at an azimuthal angle of $\phi = 22.5$ degrees from each other. The model was sting mounted onto the PSWT roll cage which allowed the roll and pitch angle of the test model to change during tunnel operation. Test model-2 contained four kulite pressure ports oriented collinearly along the windward side of model at an offset $x/D = 0.25$ inches from each other. The ogive body was sting mounted to a linear traverse system that enabled axial relocation of the model at a fixed lateral separation of $z/D = 6$ in from the ceiling inside the test section.

To qualitatively visualize the flow field, surface oil flow visualization and high-speed Schlieren/ shadowgraphy have been employed. In the present experiments, we have used a high-speed camera operating at 10kHz for shadowgraph images. Surface oil flow visualizations on the axisymmetric body were carried out using colored pigments of fluorescent dye powder mixed with two-part mineral oil.

Surface static pressure measurements were carried out using a 16-port, 10 psi range differential pressure ESP scanner. Three PSP-CCD-C (ISSI) cameras with 35mm lens and four LM2x-DM High-Intensity Air-Cooled LED UV (ISSI) lights were set up around the PSWT test section at the respective locations shown in Figures 3a- 3d. The CCD cameras were fixed normal to the optical windows of the test section aligned with the pitch and yaw axes of the ogive body. The LED UV-lights were positioned to optimize the illumination of the ogive body when captured by the cameras. The additional fourth UV-light seen in Figure 3c was installed on the camera-less +90 degree side of the test section to create an even illumination of the model. Unsteady pressure measurements were carried out using four 30 psi absolute Kulite pressure transducers.

Forces and moments were measured using a 0.5-inch diameter, 4-inch long internal strain gauge balance with appropriate load ranges to ensure a high accuracy measurement. The load ratings for the strain gage balance used in the polysonic wind tunnel are: normal force = 200 lbs, side force = 100 lbs, axial force = 50 lbs, pitching moment = 210 inch-lbs, yawing moment = 85 inch-lbs and rolling moment = 50 inch-lbs. The load balance was carefully calibrated before the wind tunnel tests, and the appropriate calibration matrix was utilized to obtain forces and moments experienced by the test model.

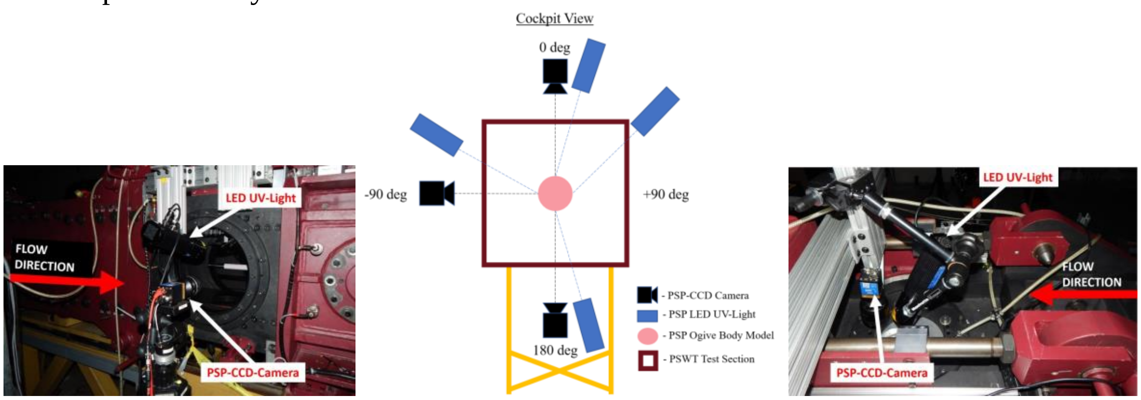

***Figure 3**: PSP setup in Polysonic wind tunnel*

3.3 Simulations

Kestrel is a multi-physics flow solver developed for the fixed wing component of the Computational Research and Engineering Acquisition Tools and Environments (CREATE) Program. Kestrel version 5.0 allows the use of a background Cartesian mesh for better resolution of flow features. Kestrel has recently introduced SAMCart, a Cartesian solver with adaptive mesh refinement, making it possible to simulate and capture the shock system. A primary advantage of Cartesian solvers is the ability to efficiently compute higher-order fluxes. Kestrel's Cartesian solver adds the ability to compute third- or fifth-order upwind fluxes to the central-difference schemes. The wind tunnel configuration was modeled with Kestrel's dual-mesh capability. The problem consists of a 10º wedge that generates a shock that impinges on the ogive body, which is at an angle of attack of 0 deg. To better capture the shock system, the shock sensor defined by

$$\phi = \frac{l(u \cdot \nabla p)}{ap}$$

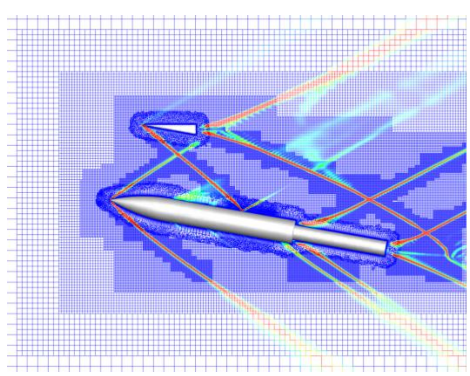

***Figure 4:** CFD Mesh simulations using Kestrel*

This was used as an adaptation variable. The sensor output φ is a non-dimensional value calculated from the dot product of velocity and pressure gradient, normalized by a reference length l, the local speed of sound a, and local pressure p. The final mesh colored by the shock sensor is shown in Fig. 4.

4. Results and Discussion

4.1 Flow visualizations

A comparison of surface oil flow visualization carried out at the PSWT and surface shear stress contours obtained using numerical simulations at Mach 2 is shown in Fig. 5. The results clearly show the shock impingement location and the shock wrapping around the body, cross-flow separation, and reattachment locations. As expected the shear stress values are low in the attached flow on the body and high at the shock impingement location. The size of the recirculating bubble appears to be very small and doesn't appear to results in significant flow separation.

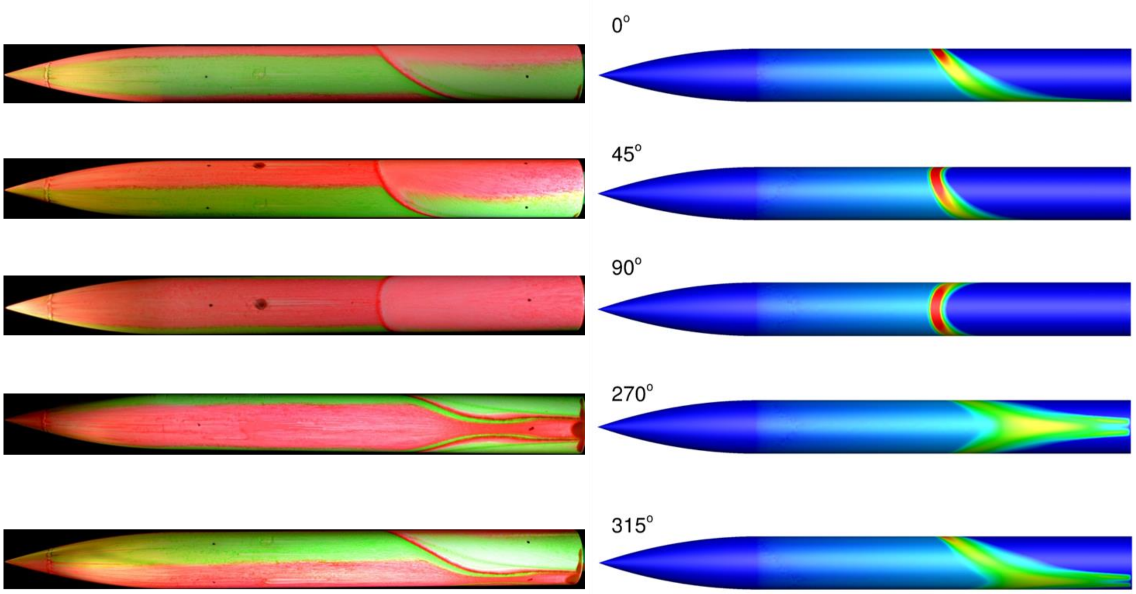

Figure 5: *Comparison of oil flow visualization from experiments and surface shear stress contours obtained using numerical simulations.*

A comparison of shadowgraph images from the experiment and numerical simulations is shown in Fig. 6. The oil flow visualization image is overlaid to aid the visualization of flow features. The shadowgraph images clearly show shocks emanating from the shock generator and the tangent ogive nose, the shock-shock interactions, and the interaction of wedge generated shock with the boundary layer on the cylindrical region of the body. The incident shock impinges on the surface and interacts with a thin boundary layer and then reflects from the surface leading to a weak interaction process. Various regions of the flow (1-6) have been identified and flow characteristics have been estimated based on gas dynamics involving shock waves. Fig. 6d shows the pressure iso-surfaces obtained using numerical simulations.

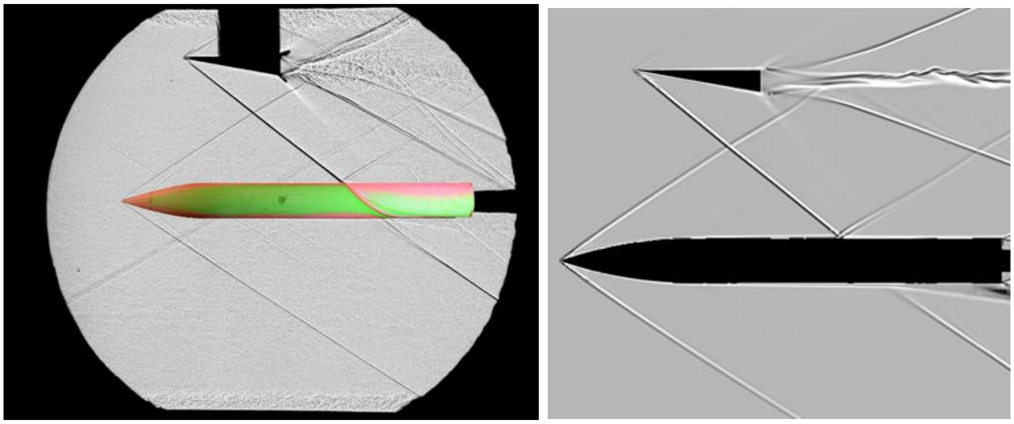

a) Experimental shadowgraph Image b) Numerical Shadowgraph Image

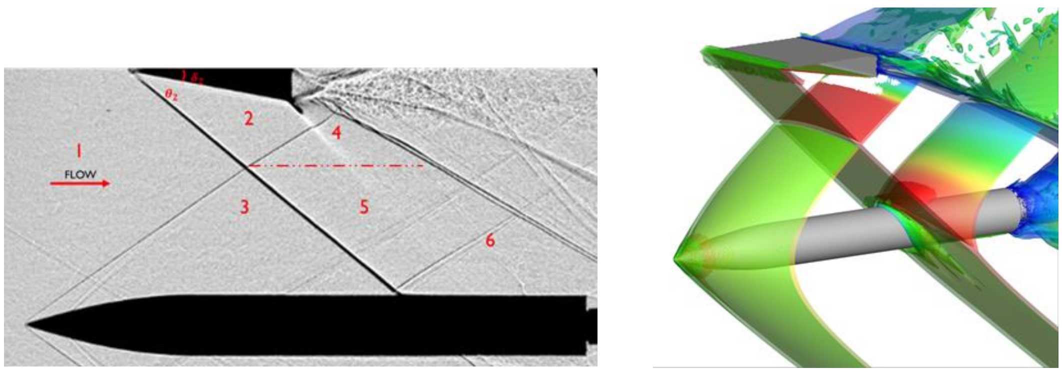

c) Shadowgraph Image Analysis d) Pressure Iso-surface

Figure 6: *Comparison of shadowgraph flow visualization from experiments and the one obtained using numerical simulations*

4.2 Surface Static Pressure Measurements

Azimuthal surface static pressure distributions at various x/D locations in the vicinity of shock-boundary layer interaction region are shown in Figure 7. The results are presented in the form of a coefficient of pressure defined as:

$$C_p = \frac{P_{static} - P_\infty}{\frac{\gamma}{2} P_\infty M^2}$$

As expected, at x/D = 6.46, a location upstream of the shock impingement (x/D = 6.65), the value of C_p is nearly zero with a small variation with azimuthal angle. The upstream influence of shock impingement is observed at x/D = 6.61. At all measurement locations, pressure peaks due to pressure jump across the shock are observed. The value of C_p peaks at x/D = 7.06 and ϕ = 0 deg and then relaxes to freestream pressure at downstream locations. The size of the separation bubble indicated by a plateau in the pressure distribution increases from the top generator to the side plane. Another interesting feature is the rise in pressure on the bottom surface at x/D>7.51.

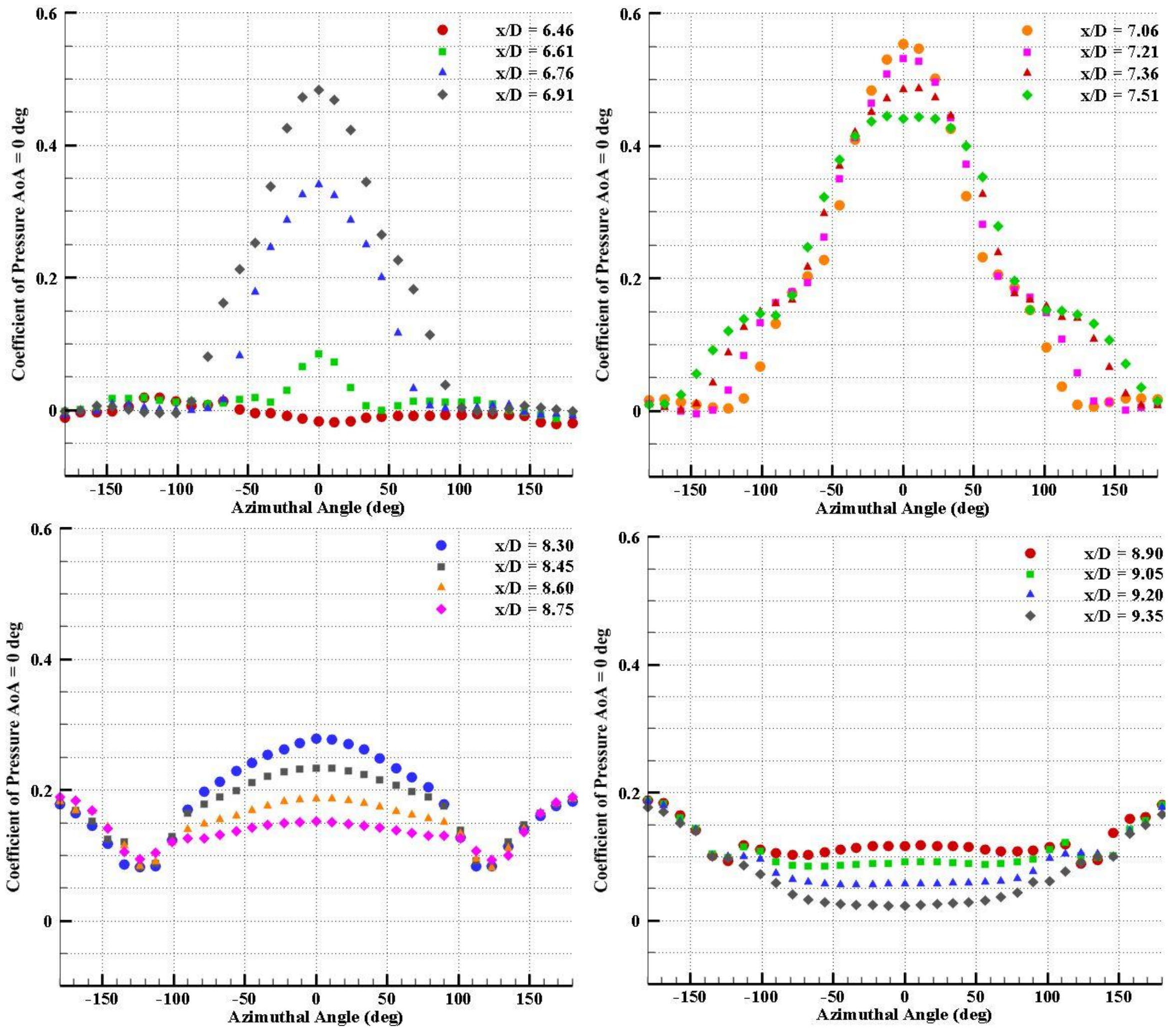

Figure 7: *Azimuthal surface static pressure distributions around the cylindrical body in the vicinity of SBLI.*

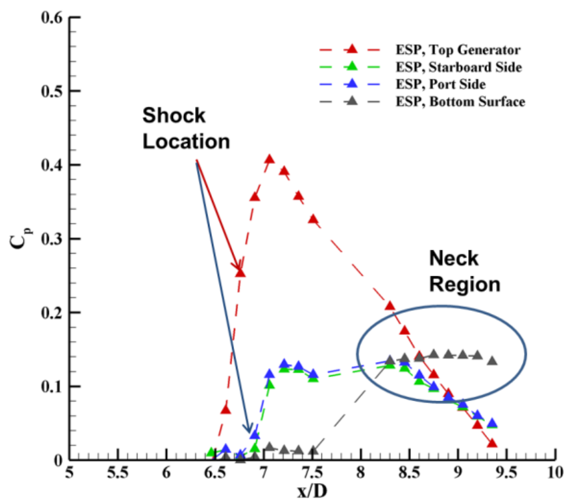

Figure 8: *Surface static pressure distributions along the cylindrical body in the vicinity of SBLI.*

The longitudinal surface static pressure distributions in the vicinity of shock-boundary layer interaction region are shown in Figure 8. The pressure jump across the shock on the top generator is much higher than that on the side indicating the strength of shock experienced by the top surface is much higher than the side due to the size of the separation bubble. The pressure distributions on the sides are identical indicating the model and shock symmetry. The value of Cp = 0 on the bottom surface up to x/D = 7.5 indicating attached flow. An increase in pressure for x/D > 7.5 on the bottom surface is due to the neck formation/convergence and divergence of supersonic flow as observed in surface flow features (Figure 5).

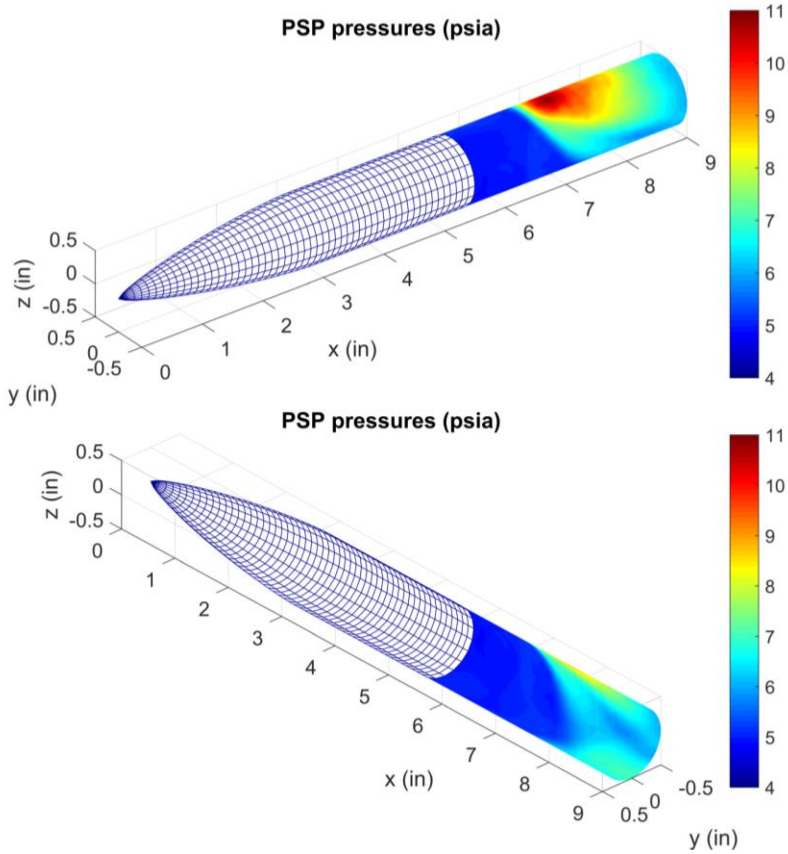

Figure 9: *Surface static pressure field in the vicinity of SBLI measured using PSP*

To obtain a surface static pressure field in the vicinity of shock-boundary layer interaction region pressure sensitive paint technique was utilized. The data obtained using three camera views was processed and used for reconstruction of the 3-dimensional pressure field around the axisymmetric body. Unlike surface static pressures obtained using ESP at discrete locations, the PSP pressure field has millions of pressure points and provide rich information about the pressures in the SBLI region. A comparison of pressure distribution along the four generators obtained using ESP and PSP is shown in Figure 10. The results clearly show an excellent agreement between the two measurement techniques. The data obtained using PSP clearly fills the gaps between pressure distribution obtained using ESP.

The pressure field on the axisymmetric body was also simulated using Kestrel and the results are shown in Figure 11. The pressure field shows the regions of high and low pressures, in particular, the pressure jumps in the vicinity of shock-boundary layer interactions. A comparison of pressure distribution obtained using Kestrel with ESP and PSP data show good results. Kestrel picks up the shock location well, however, predicts a slightly higher pressure peak. The pressure predicted on the two sides matches well with the data, however, pressure distribution predicted on the bottom surface show some differences, which require further investigation.

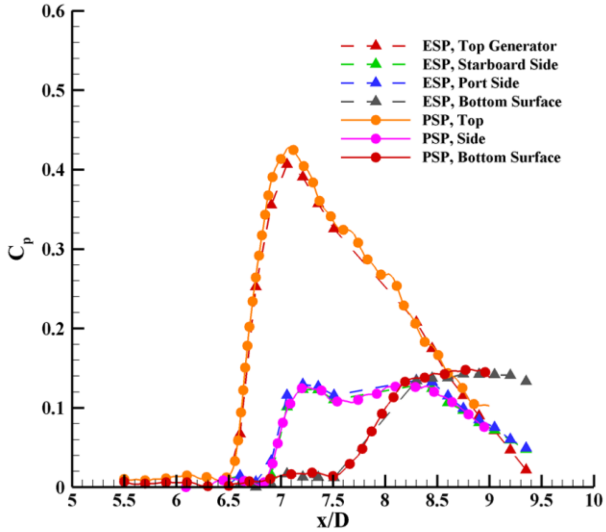

Figure 10: *Comparison of surface static pressure distributions obtained using ESP and PSP*

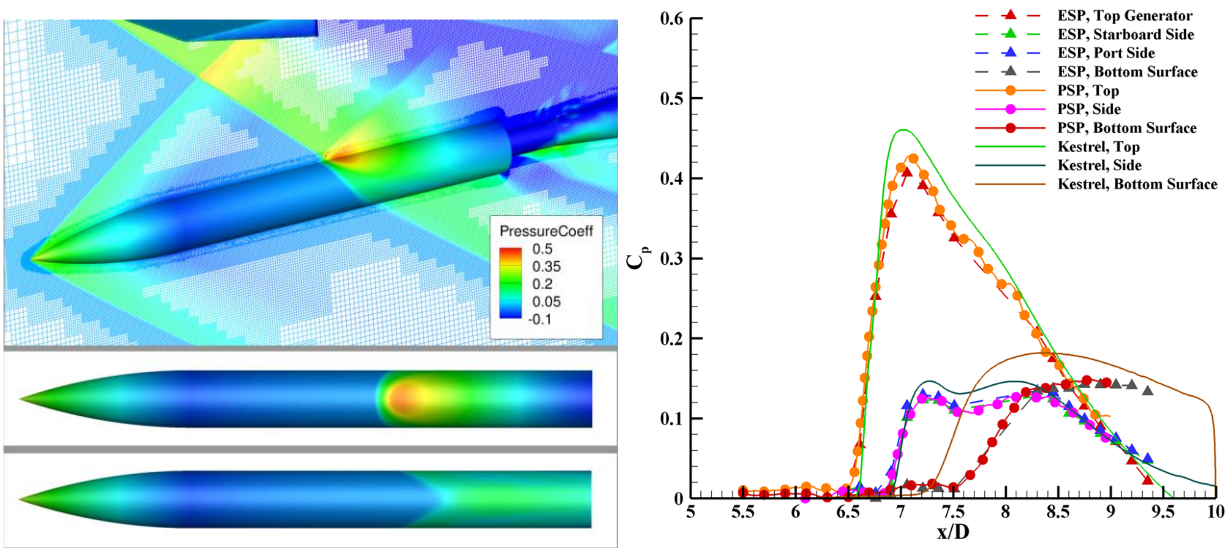

Figure 11: *Surface static pressure field obtained using Kestrel.*

4.3 Unsteady Surface Pressures

Surface pressure fluctuations were measured using fast-response Kulite pressure sensors. Figures 12 – 14 illustrate the normalized pressure spectra on the ogive cylinder body, and the surface flow features with respect to the regions where pressure fluctuations were measured. The axial coordinate system implemented designates the windward impinging shock foot as the origin ($x_s/D = 0$), where x_s is the streamwise distance between the shock foot and the pressure sensor, and D is the model diameter.

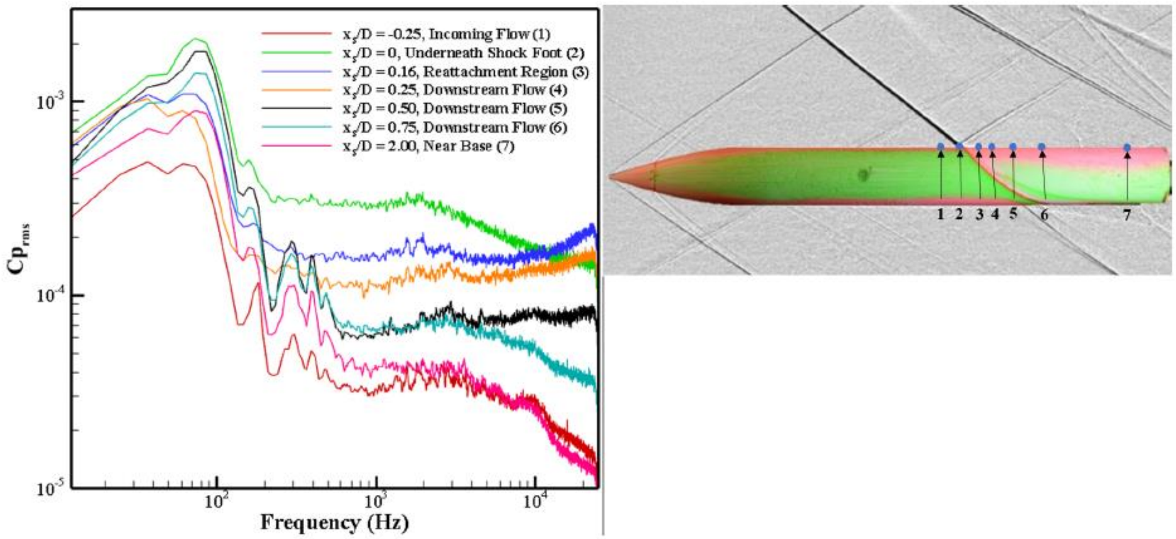

Figure 12: *Surface pressure fluctuation spectra of the SBLI region ϕ = 0°.*

At ϕ = 0° (windward), as expected pressure fluctuations are minimum in the incoming flow (x_s/D = -0.25) corresponding to turbulent boundary layer, and maximum beneath the shock impingement location. The shock spectra (x_s/D = 0) is characterized by high amplitude low frequency oscillations (f = 75Hz), followed by a plateau in the middle (200Hz to 1kHz) and a decrease in energy at high frequencies (>1kHz). In the reattachment region (x_s/D = 0.16), the spectra shows high-amplitude low-frequency oscillations followed by nearly constant energy fluctuations over the entire frequency range, except for a small increase seen at very high frequencies (>10kHz). The spectra measured far downstream of shock impingement finally relaxes back to incoming flow levels. Small peaks observed at 150Hz and 300Hz correspond to model natural frequency and its harmonics. The absence of these peaks over the range f = 150Hz to 300Hz in the spectra of the shock foot (x_s/D = 0) and reattachment region (x_s/D = 0.16) is due to the elevated energy fluctuation causing the peaks to be dampened.

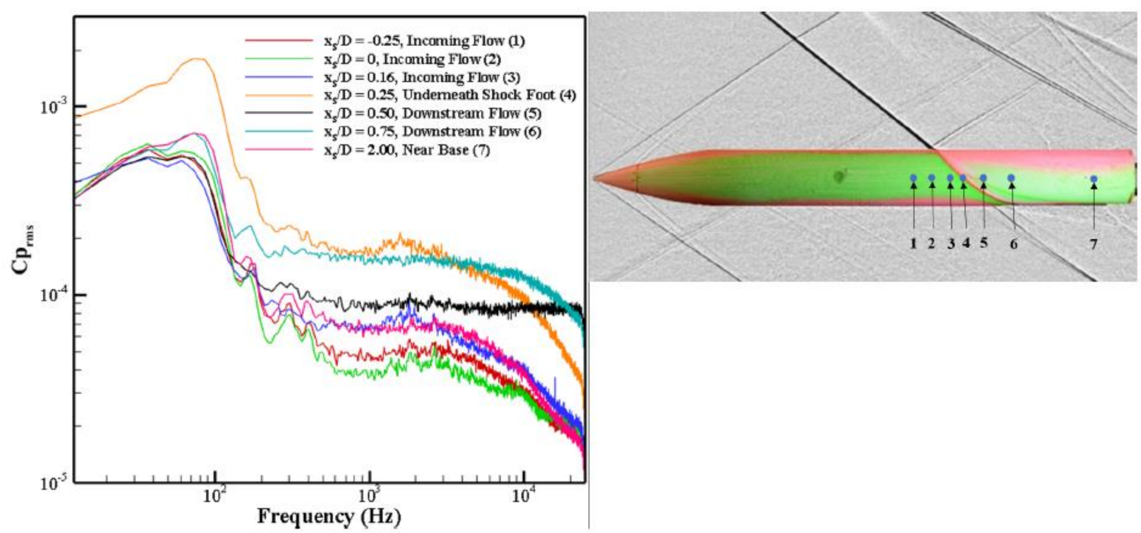

Figure 13: *Surface pressure fluctuation spectra of the SBLI region ϕ = 90°.*

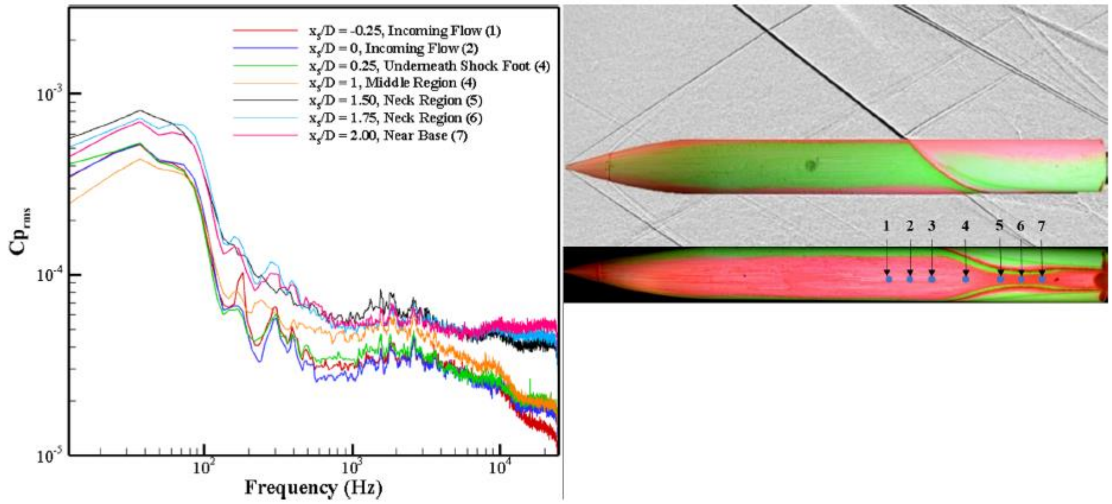

Figure 14: *Surface pressure fluctuation spectra of the SBLI region ϕ = 180°.*

The maximum pressure fluctuations seen in the spectra of figure 13, in correspondence to the oblique shape of the impinging planar shock, indicate that the location of the shock foot at ϕ = 90° (side generator) is shifted downstream (x_s/D = 0.25). Due to the shock shift, the pressure fluctuations captured beneath the shock (x_s/D = 0) at ϕ = 0° corresponds with the smallest pressure fluctuations of the incoming flow, resultant of the turbulent boundary layer. Consistent with the flow behavior on the windward side of the model, the spectra underneath the shock (x_s/D = 0.25) is characterized by high amplitude unsteadiness at low frequencies (f = 75Hz), a near plateau mid-region (200Hz to 1kHz), and a decrease in energy at high frequencies (>1kHz). Unlike that seen at ϕ = 0° (windward side), the low frequency pressure fluctuation amplitudes upstream and downstream the shock foot are similar in magnitude showing no incremental decline. The pressure fluctuation of the plateau mid-region (200Hz to 1kHz) downstream the shock foot shows a decrease in energy fluctuations (x_s/D = 0.50) followed by an increase in fluctuations (x_s/D = 0.75). This behavior deviates from ϕ = 0°, where unsteadiness amplitudes consistently decrease with increase in distance downstream and is attributed to the pressure fluctuations (x_s/D = 0.50) measured within the growing region of separation. The elevation in energy observed (x_s/D = 0.75) is an attribute of the unsteadiness of reattached flow aft the region of separation.

At ϕ = 180° (leeward generator), the pressure fluctuations behave as the incoming flow seen at ϕ = 0° and 90°. The absence of a maximum peak at low frequency is expected as the surface flow visualization in figure 14 shows that the wrapping shock does not intersect the ϕ = 180° (leeward generator) side. The pressure fluctuations are characterized by the maximum broadband peaks seen at low frequencies. Elevated oscillations in the necking region (x_s/D = 1.50) is a result of the unsteadiness from the presence of the shock converging leeward. The spectra at very high frequency (>10kHz) in the incoming flow decreases in energy and the corresponding spectra in the neck region continue to possess high unsteadiness levels.

4.4 Force and Moment Measurements

Force measurements were carried out at Mach 2 at the PSWT. The objective of these tests was to study the effect of shock impingement location on the aerodynamic characteristics of the ogive cylinder body at supersonic speeds. During force measurements, the body was translated along the streamwise direction using captive trajectory system integrated with the PSWT to alter the shock impingement location. The wedge was positioned such that its leading edge lateral separation from the ogive nose tip was a constant z/D = 4.327 while the axial distance between its leading edge and the ogive nose varied during the tests (Fig. 15). A total of five shock impingement locations were selected to evaluate the effects of an axisymmetric body axially traversing through a supersonic flow field. The tests were carried out with and without a shock generator. The results are shown in Fig. 15. As expected both the normal force and pitching moment coefficient values are zero for the body alone (no shock generator) at zero deg angle of incidence. In the presence of a shock generator, the shock impingement on the body results in a negative normal force for the range of x/D tested. The value of the normal force coefficient varies with the shock impingement location and the variation is linear. The location of shock impingement with respect to the center of pressure is expected to affect the pitching moment coefficient and the results are clearly visible in Fig. 15.

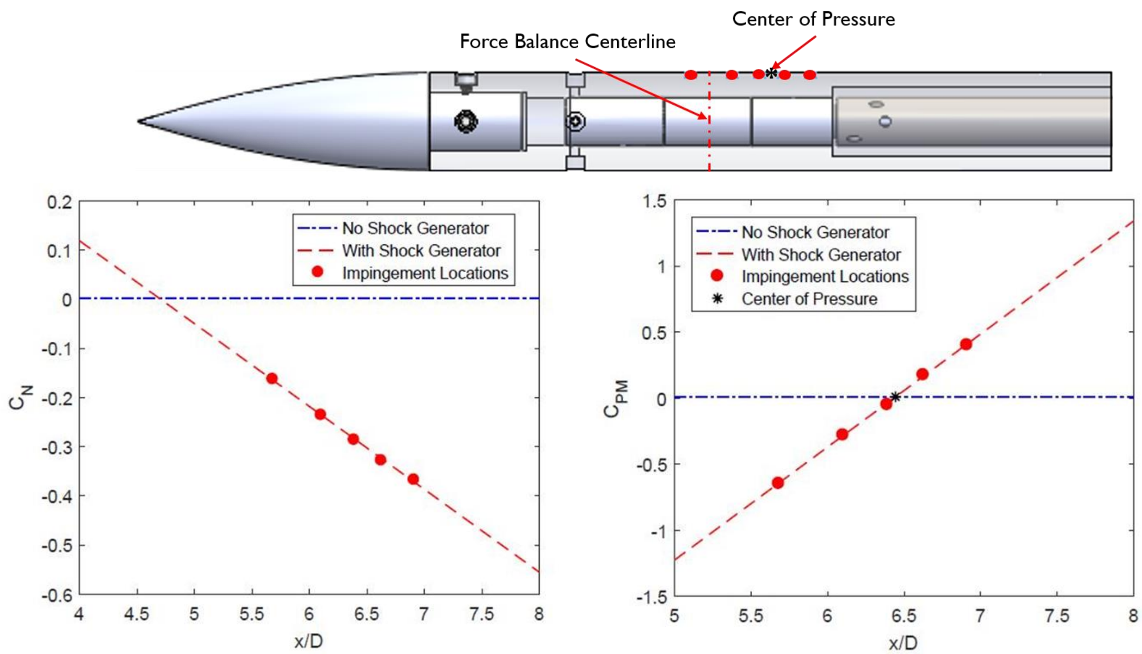

Figure 15: *Aerodynamic characteristics of the axisymmetric body with and without shock impingement.*

Interactions/Transitions

1. Mason, F., Natarajan, K., and Kumar, R., "Shockwave Boundary Layer Interactions on an Axisymmetric Body at Mach 2", *Accepted for publication in AIAA Journal*.
2. Mason, F., Kumar, R. and Eymann, T., "Shock Boundary Layer Interaction Induced Surface Pressure Field on an Axisymmetric Body", AIAA SciTech Forum, 6-10 January 2020, Orlando, FL, *AIAA 2020-0570.*
3. Mason, F., Kumar, R., "Shock-Wave-Boundary-Layer Interactions on an axisymmetric Body", 131st Supersonic Tunnel Association International (STAI) Meeting, 12-15 May 2019, Bangalore, India.

4. Mason, F., Kumar, R. and Eymann, T., "Study of Impinging Planar Shock Wave Boundary Layer Interactions on an Axisymmetric Body", AIAA SciTech Forum, 7-11 January 2019, San Diego, CA, *AIAA 2019-0342*.
5. Fraeman Mason participated in the Kestrel CREATE-AV and Capstone training session on June 11-14, 2018 in California, Maryland.

Acknowledgment/Disclaimer

This work is supported by the Air Force Office of Scientific Research, USAF, under AFOSR Grant number FA9550-17-1-0269. The views and conclusions contained herein are those of the authors and should not be interpreted as necessarily representing the official policies and endorsements, either expressed or implied, of the Air Force Office of Scientific Research or the U. S. Government.